Desalination and Water Treatment
www.deswater.com

doi: 10.1080/19443994.2014.984767

57 (2016) 3559–3571
February

Taylor & Francis
Taylor & Francis Group

Nanoscale iron oxides loaded granular activated carbon (GAC-NSIO) for cadmium removal

Zhihua Xu, Daofang Zhang*, Weifang Chen, Yaru Li, Shijue Yuan

Department of Environmental Science and Engineering, School of Environment and Architecture, University of Shanghai for Science and Technology, Shanghai 200093, PR China, Tel. +86 13585627276; Fax: +86 2155275979; email: leon_xu0812@163.com (Z. Xu), Tel. +86 13701780711; Fax: +86 2155275979; email: dfzhang_usst@163.com (D. Zhang), Tel./Fax: +86 2155275979; email: chenzjzj@gmail.com (W. Chen), Tel. +86 2155270697; Fax: +86 2155275979; emails: lyrhgd_sz@163.com (Y. Li), 13681990676@163.com (S. Yuan)

Received 8 April 2014; Accepted 31 October 2014

ABSTRACT

A new hybrid material was prepared by loading the nanoscale iron oxide particles within the pores of granular activated carbon (GAC-NSIO) and used as adsorbent to remove Cd(II) in aqueous phase. The new material is characterized by the pH_{pzc}, TEM, XRD, BET, and XPS analytical techniques to deduce the potential adsorptive mechanism, and further it along with GAC were assessed in the removal of Cd(II) from aqueous solution for various physico-chemical factors iron-loaded content, pH, humic acid, isotherm, kinetics, and thermodynamics, under the batch reactor studies and rapid small-scale column tests also appended dealing with the breakthrough volume. Characterization of adsorbent indicated that the amorphous nanoscale iron oxides were successfully immobilized on GAC. Adsorption mechanism mainly included surface complexation, Donnan membrane effect, and electrostatic attraction. The optimum iron-loaded content of GAC-NSIO was 17%. The adsorption process was more favorable at high pH, and iron oxide was almost no leaching (<0.25%) in the pH range of 3–6. Adsorption isotherm fitted well with Langmuir and Freundlich models. And adsorption kinetics fitted well with pseudo-second-order and intraparticle diffusion models. Results indicated that loaded nanoscale iron oxides significantly increased adsorption capacity of Cd(II) though the adsorption rate declined slightly and the adsorption process was endothermic. The maximum adsorptive capacity of GAC-NSIO (7.84 mg/g) increased by 700%, compared to that of GAC (0.98 mg/g). The presence of humic acid could greatly impact Cd(II) adsorption which promoted adsorption at low concentrations (1–10 mg/L) and inhibited adsorption at high concentrations (10–300 mg/L). Rapid small-scale column tests were conducted to obtain Cd(II) breakthrough profile. The results corresponded well with those from batch tests. Results demonstrate that the GAC-NSIO is a promising adsorbent for the removal of Cd(II) in contaminated water environment.

Keywords: Cadmium; Nanoscale iron oxides; Activated carbon; Adsorption

*Corresponding author.

1. Introduction

With the rapid development of industrial activities, massive toxic heavy metals were discharged into various aqueous bodies, giving rise to critical environment problems [1]. As an important heavy metal, cadmium was usually found to be discharged from industries such as cadmium plating, Ni–Cd batteries, copper alloys, and paint pigment [2,3]. Cd(II) is recognized as a potential human carcinogen [4]. Long-term exposure to Cd(II) could induce some serious diseases (osteomalacia, osteoporosis, renal dysfunction, or hormone change) to human body even at lowlevel [5,6]. Permissible limit of Cd(II) in drinking water recommended by the USEPA was 0.005 mg/L [7]. In 2006, China established a maximum contamination level (MCL) of 0.005 mg/L for Cd(II).

Conventional treatment technologies for heavy metals mainly include chemical precipitation [8], ion-exchange [9], adsorption [10], membrane [11], flotation [12], coagulation–flocculation [13], and electrochemical methods [14]. Among these, adsorption process is featured by its easy setup, simple operation, low maintenance cost, and many types of readily accessible cost-effective adsorbents.

Recently, nanoscale iron (hydr)oxides have been widely used as adsorbents for the removal of heavy metals in aqueous environment. The utilization of iron oxide nanomaterials as adsorption materials and photocatalysts have been received much attention as to their special properties, such as extremely small size, huge specific surface area, high surface energy, surface modifiability, excellent magnetic performance, and good compatibility [15–18]. However, they are very fine and easy to form agglomeration thus are difficult to implement in solid–liquid separate process, so their engineering applicability is often limited [19]. It was also difficult to employ them in a fixed bed or flow through regime due to their low mechanical strength and excessive pressure buildup. In order to improve the application of nanoscale iron (hydr)oxides, it is an innovative research point that impregnating them into porous materials of bulk size to obtain hybrid adsorbents [15,20,21]. Granular activated carbon (GAC) as a porous substance has some excellent merits of high specific surface area, abundant chemical functional groups, good mechanical strength, and acid–alkali resistance and has been widely used for removal of organic pollutants. Some scholars have researched the utilization of GAC to remove heavy metals from aqueous solution, but it had only relatively small adsorption property and weak affinity for heavy metals [22].

In this study, GAC was investigated as the carrier of nanoscale iron oxides. The goal was to take full advantages of both high affinity of nanoscale iron oxides for heavy metals and the structure and chemical merits of GAC by impregnating nanoscale iron oxides into GAC. And abundant pore structure and high specific surface area of GAC have been proved to be able to supply effective active sites for loading nano particles [23]. Combination of nanoscale iron oxides and GAC is considered to be a very potential orient for adsorption of heavy metals. At present, many researchers mainly focused on heavy metal anions removal in aqueous, such as Cr(VI), AS(V) [24–27], few literatures discussed on the removal of Cd(II), and little was known on the adsorption capacity and mechanism. The contents of this research were to prepare and evaluate a new nanoscale iron oxides loaded GAC for the removal of Cd(II). Adsorption isotherm, kinetics, thermodynamics, and rapid small-scale columns tests were carried out to test the adsorption capacity, rate, energy of adsorption, and breakthrough profile. The adsorption mechanism was discussed to explain the adsorption phenomenon. The effects of pH, iron content, and humic acid were also investigated in details.

2. Materials and methods

2.1. Materials and chemicals

Coal-based GAC was obtained from Shanghai Xing Chang Activated Carbon Co. Ltd, China. All chemicals were of analytical grade without further purification and were purchased from China Chemicals Inc. Milli-Q element ultrapure water (18.2 Ω, Millipore, Billerica, MA, USA) was used throughout the experiment.

2.2. Preparation

The nanoscale iron oxides loaded granular activated carbon (GAC-NSIO) was synthesized according to the method based on Chen and Li [28]. The preparation of GAC-NSIO consists of six steps: (1) The GAC was ground and sieved to US mesh size 100 × 200, which was added into boiled ultrapure water for 2 h and then put into ultrasonic cleaner for 1 h at power of 90 W to remove impurities and ash content. After that, GAC was washed by ultrapure water for 3–5 times and dried in oven at 373 K for 12 h. (2) Ten grams of GAC was added to 1 L of 1 mol/L NaOH solution in a 2-L Erlenmeyer flask and then was mixed fully by the magnetic stirrer for 0.5 h. (3) 12.5 g (25 g or 50 g) of $Fe_2(SO_4)_3$ was added to the mixture then put on a shaker at 298 K for 4 h. (4) The mixture was poured into the sealed polyethylene bottle, which was heated in an oven at 313 K for 48 h. (5)

GAC-NSIO was separated from the mixture by filter sieve (400 mesh) and washed thoroughly by ultrapure water until neutral pH in order to get rid of loose nanoscale iron oxides. (6) Solid particles were desiccated at 373 K for 12 h and sealed prior to use. For example, the GAC loaded with 17% mass content of iron and the non-loaded GAC were named as GAC-NSIO(17%) and virgin GAC, respectively.

2.3. Batch experiment

500 mg/L Cd(II): 0.93 g $CdSO_4$ was dissolved by 1L milli-Q ultrapure water to Cd(II) stock solution. 0.05–50 mg/L Cd(II): Different Cd(II) concentrations (0.05–50 mg/L) were prepared by diluting Cd(II) stock solution (500 mg/L) with different multiple (10–1,000).

2.3.1. Adsorption isotherm and effect of pH

Adsorption isotherm experiments were conducted at 298 K with a shaking speed of 150 rpm. 0.1 g of adsorbent was added to 100 mL of solution with different Cd(II) concentrations (0.05–50 mg/L). The adsorption equilibration time was 24 h. The sorption data were fitted to Langmuir and Freundlich isotherm models [29] as shown in Eqs. (1) and (2).

$$q_e = q_m \frac{bC_e}{1 + bC_e} \tag{1}$$

where q_e is the equilibrium adsorption capacity (mg/g), C_e is the equilibrium concentration of solution (mg/L). q_m and b are constants. q_m is the maximum adsorption capacity (mg/g) and b is the Langmuir constant related to the free energy of capacity (L/mg).

$$q_e = K_f \times C_e^{1/n} \tag{2}$$

where q_e is the equilibrium adsorption capacity (mg/g), C_e is the equilibrium concentration of solution (mg/L). K_f and n are indicative isotherm parameters of adsorption capacity and intensity, respectively.

Adsorption isotherm experiments were also carried out at different pH (3–6) to study the effect of pH. The value of pH was adjusted by 0.1 mmol/L NaOH or HCl solutions.

2.3.2. Effect of contact time

Effect of contact time was carried out at 298 K and 150 rpm. 0.1 g of adsorbent was added to 16 Erlenmeyer flasks each containing 100 mL of 1 mg/L Cd(II) solution at pH 6.0. The adsorption time were set to be 0, 20, 40, 60, 90, 120, 180, 240, 360, 480, 600, 720, 900, 1,080, 1,260, and 1,440 min, when the reaction ended, the sample was filtered by 0.45 μm filter. The process of adsorption was described by pseudo-first-order and pseudo-second-order models [30] as shown in Eqs. (3) and (4).

Pseudo-first-order kinetic model:

$$\log(q_e - q_t) = \log q_e - \frac{k_1}{2.303} t \tag{3}$$

Pseudo-second-order kinetic model:

$$\frac{t}{q_t} = \frac{1}{k_2 q_e^2} + \frac{1}{q_e} t \tag{4}$$

where q_e and q_t are Cd(II) adsorption capacity at equilibrium and time t (mg/g). k_1 is the adsorption rate constant of pseudo-first-order (1/min) and k_2 is the adsorption rate constant of pseudo-second-order (g/mg min).

In adsorption systems, there is the possibility of intraparticle diffusion being the rate-limiting step, the intraparticle diffusion model [30] is shown in Eq. (5).

$$q_t = K_d t^{0.5} + C \tag{5}$$

where K_d is the rate constant of intraparticle diffusion (mg/g $\text{min}^{0.5}$) and C is the intercept (mg/g).

2.3.3. Effect of temperature

0.1 g adsorbent was added to 100 mL of solutions with different concentrations of Cd(II) (0.05–50 mg/L) at 288 K, 298 K and 308 K, respectively. The thermodynamic parameters, such as standard enthalpy (ΔH°), Gibbs free energy (ΔG°), and entropy (ΔS°), were calculated using the Eqs. (5) and (6) [30]:

$$\Delta G^\circ = -RT \ln K_L \tag{6}$$

$$\ln K_L = \frac{\Delta S^\circ}{R} - \frac{\Delta H^\circ}{RT} \tag{7}$$

where K_L is the distribution coefficient for the adsorption process, it can be determined by the Langmuir constant b (L/mol) at different temperatures. T is temperature (K). ΔG°, ΔH°, and ΔS° are the change of Gibbs energy, enthalpy, and entropy. R is the gas constant (8.314 J/mol K). The value of ΔH° and ΔS° could be obtained by the slopes and intercepts of plot of ln K_L against $1/T$.

2.3.4. Effect of humic acid

Humic acid (sodium salt, 50–60%, Ourchem) was purchased from China Chemicals Inc. The CAS no. is 68131-04-4, and the molecular formula is $C_9H_8Na_2O_4$, whose molecular weight is 226. 0.1 g of adsorbent was added to 100 mL of solution containing 0.1 mmol/L (11.24 mg/L) of Cd(II) which were spiked with 5, 10, 30, 100, 150, 200, and 300 mg/L of humic acid, respectively. The mixture was equilibrated for 24 h, and the sample was filtered by 0.45 μm filter.

2.4. Rapid small-scale column tests

A schematic diagram for the rapid small-scale column tests (RSSCT) is shown in Fig. 1. RSSCT were carried out with a polymethyl methacrylate column (diameter: 0.5 cm, length: 13.5 cm) by a constant downflow configuration to maintain an empty bed contact time (EBCT) of 0.6 min. Influent concentration of Cd (II) was kept constant at 1 mg/L under pH 6.0. The plunger pumps (Shanghai Tauto Biotech Co. Ltd., China) were used to ensure a constant rate.

2.5. Characterization

The specific surface area and pore size distribution of adsorbents were determined using N_2 adsorption and desorption tests at 77 K (Micromeritics ASAP-2020, USA). The adsorbents were observed with transmission electron microscopy (Hitachi Model H-800, Japan). Crystal structure of adsorbent was determined by powder X-ray diffraction patterns over a wide range of angles from 10° to 90° using a high-resolution X-ray diffraction (Bruker D8,Germany) with Cu Kβ. X-ray photoelectron spectroscopy of the given samples were made with a spectroscopy (ESCALAB-2, Great Britain) equipped with an Mg Kα X-ray source (1253.6 eV protons). pH_{pzc} of all samples were conducted by the method recommended by Noh and Schwarz [31]. One gram of sample was added to 10 mL of milli-Q ultrapure water, and the mixture was then put on a shaker (150 rpm, 298 K) for 24 h. The equilibrium pH of suspension was measured and equivalent to pH_{pzc}.

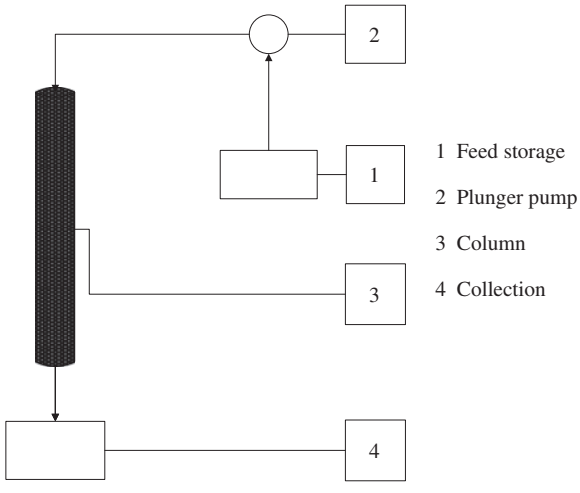

Fig. 1. Experiment system for rapid small-scale column tests (RSSCT). (1) Feed storage; (2) plunger pump; (3) column; (4) collection.

2.6. Analytical methods

Concentrations of all heavy metal ions were measured by an atomic absorption spectrophotometer (AAS, TAS-990, PERSEE) or inductively coupled plasma mass spectrometry (ICP-MS, 300X, PE). To determine the iron-loaded content, GAC-NSIO was calcined in muffle furnace at 873 K for 2 h and the resultant ash was dissolved in 2 mol/L HCl (25 ml) for 24 h. Concentration of iron was analyzed, and iron content could be calculated.

3. Results and discussion

3.1. Adsorption isotherm and optimization of iron-loaded content in GAC-NSIO

According to preparation method, we successfully prepared the adsorbents with different iron content. Adsorption isotherm tests were first conducted to screen the iron-oxide loading GAC. The iron content and adsorption isotherms constants of different adsorbents are shown in Table 1.

The amount of loaded iron had significant effect on Cd(II) adsorption. Isotherms data of different adsorbents all fitted well with both Langmuir isotherm model and Freundlich isotherm model. The correlation coefficients (R^2) are between 0.90 and 0.99. Langmur q_{max} and Freundlich K_f both revealed that the Cd(II) adsorption capacity followed the order of GAC-NSIO(17%) > GAC-NSIO(27%) > GAC-NSIO (10%) > virgin GAC.

The increase in adsorption may be attributed to the extra sites provided by iron oxides. However, the extent of enhance is not proportional to the amount of iron loading. GAC-NSIO(17%) exhibited the highest adsorption property. This interesting finding might due to the reason that the excessive NSIO particles on the surface and in the pores of GAC led to aggregation of the nanoscale chemicals, causing the decrease of amount of active adsorption sites and reduction of adsorption capacity [19]. Moreover, BET surface area

Table 1
Iron-loaded content of adsorbents and their adsorption isotherms constants

Adsorbent	Iron-loaded content (%)	Langmuir isotherm model			Freundlich isotherm model		
		q_{max} (mg/g)	b (L/mg)	R^2	K_f (mg/g)	$1/n$	R^2
Virgin GAC	0	0.98	0.90	0.99	0.47	0.27	0.93
GAC-NSIO(10%)	10	4.23	0.82	0.99	2.23	0.23	0.90
GAC-NSIO(17%)	17	7.84	0.17	0.95	2.44	0.28	0.96
GAC-NSIO(27%)	27	5.07	0.51	0.98	2.00	0.36	0.90

of virgin GAC and GAC-NISO(27%) are 1,103 and 877 m^2/g, and the excessive reduction of specific surface area might lower the adsorption capacity of Cd(II).

3.2. Characterization

Since GAC-NISO(17%) manifested the highest adsorption of Cd(II). All following tests were focused and in comparison with virgin GAC.

The results of the pore size distribution analysis are shown in Fig. 2. Compared with virgin GAC, the decrease of pore volume along with variety of pore distribution were observed in GAC-NSIO(17%).

Table 2 compares the pore volume distribution of the GAC before and after iron loading. The data of these pore volume had been converted to per gram of GAC rather than per gram of the adsorbent. Compared with virgin GAC, the decrease of pore volume mainly appeared in the range of pore sizes from 2 to 10 nm for GAC-NSIO(17%).

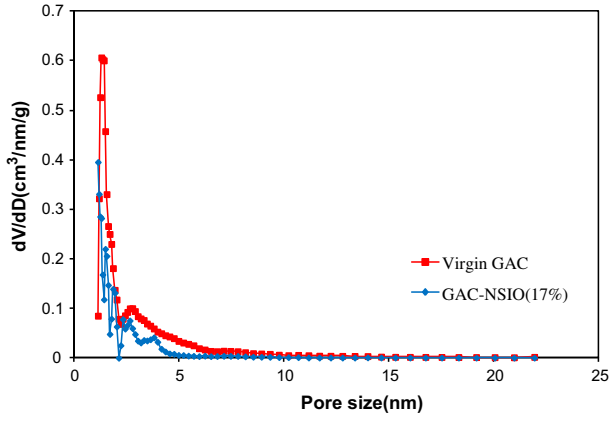

Fig. 2. Pore size distributions curve of virgin GAC and GAC-NSIO(17%).

This result proved that most of the iron oxides had been successfully loaded as nanoparticles with width between 2 and 10 nm. The obvious increase in pore volume of pore sizes from 1 to 2 nm for GAC-NSIO (17%) was observed because the pores of GAC wider than this range had been doped with iron oxides thus formed smaller pore size. Assuming NSIO at all pore sizes having the same density and the change of pore sizes were only due to the iron loading. The fraction of total NSIO(%) that were doped in the range of all pore sizes is also listed in Table 2. The overall difference of pore volume between virgin GAC and GAC-NSIO(17%) is 0.054 cm^3/g. And more than 90% of the iron loading appeared in the range of pore sizes from 2 to 10 nm.

TEM micrographs of prepared materials are presented in Fig. 3 (left) and (right). Comparison between images of the virgin GAC and GAC-NSIO(17%) manifested that they had the similar morphology. In Fig. 3(left), the virgin GAC had coarse and polyporous surface, providing the high specific surface area for iron oxide doping. In Fig. 3(right), nanoscale iron oxides were observed as dark area uniformly appeared in the pore structure of GAC. Obviously, the iron oxides particles were nanoscale, with a size range of 2–30 nm.

The XRD patterns of virgin GAC and GAC-NSIO (17%) are shown in Fig. 4. Virgin GAC reveals very characteristic and obvious diffraction peaks at the 2θ

Table 2
Comparison of pore volume and NSIO distribution on virgin GAC and GAC-NSIO(17%)

Pore size (nm)	Virgin GAC (cm^3/g)	GAC-NSIO(17%) (cm^3/g)	Difference (cm^3/g)	Percent of NSIO loaded (%)
1–2	0.32	0.39	−0.07	–
2–5	0.2	0.12	0.08	64.5
5–10	0.06	0.024	0.036	29.0
>10	0.03	0.022	0.008	6.5

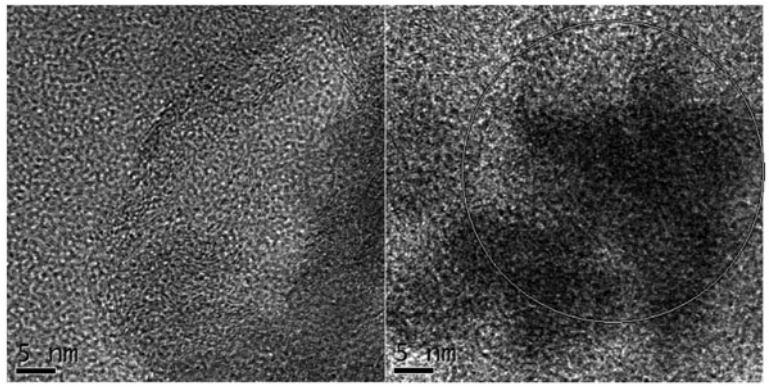

Fig. 3. TEM images of (left) virgin GAC and (right) GAC-NSIO(17%).

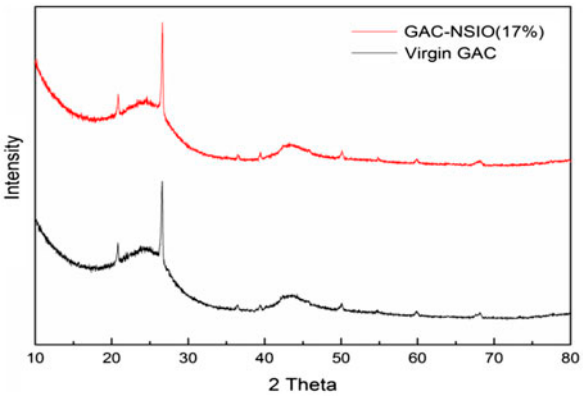

Fig. 4. XRD patterns of virgin GAC and GAC-NSIO(17%).

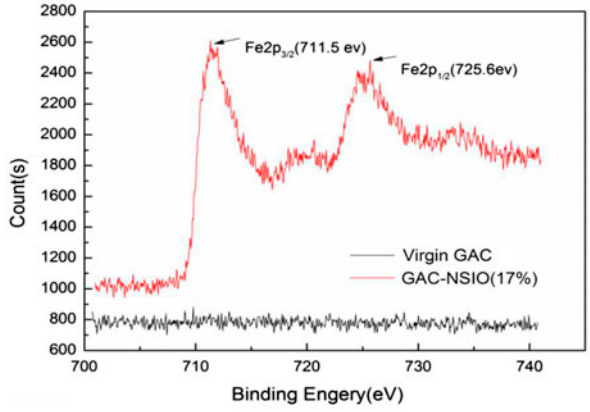

Fig. 5. XPS patterns of virgin GAC and GAC-NSIO(17%): individual XPS Fe2p binding energy region.

values of 20.859, 26.639, 36.543, 39.464, 50.138, 54.873, 59.958, 68.316, etc. These crystallized peaks (quartz) represented the presence of SiO_2 according to Joint Committee on Power Diffraction Standards (JCPDSs), which were characteristic diffraction peaks for coal-based GAC [25]. For the GAC-NSIO(17%), there is no notable change in the diffraction peaks but obvious change in the intensity of peaks. The possible reasons may included the following: (1) the doped nanoscale iron oxide was amorphous and no crystalline phases had been injected into the pores and surface of the GAC; (2) the nanoparticles were too small to diffract; (3) the concentration of doped iron oxide was too low [4,32–35].

Fig. 5 shows results of XPS analysis for Fe2p spectra between virgin GAC and GAC-NSIO (17%). The core levels are split into the $2p_{3/2}$ and $2p_{1/2}$ components due to spin-orbit coupling. In virgin GAC, there are no $Fe2p_{3/2}$ and $Fe2p_{1/2}$ peaks observed due to no existence of iron or iron oxide in GAC. In contrast, in GAC-NSIO(17%), $Fe2p_{3/2}$ and $Fe2p_{1/2}$ peaks obviously existed at ~711.5 eV and ~725.6 eV, which demonstrated that iron was completely oxidized to Fe(III). The absence of an Fe(II) component and its associated shake-up features further indicated the complete oxidation of iron [36,37]. This result manifested that nanoscale iron oxides mainly exited in form of goethite, akaganeite, hematite, maghemite, and amorphous HFO [20,37], which was confirmed by the results of XRD.

3.3. Effect of pH

Adsorption isotherms of virgin GAC and GAC-NSIO(17%) at different pHs are shown in Figs. 6 and 7, respectively. Table 3 lists the Langmuir and Freundlich adsorption constants.

Adsorption capacity increased with the increase of pH for both adsorbents, which showed that the adsorption process was pH dependent and well favored at high pH. pH_{pzc} is defined as the pH when the net surface charge of adsorbent equals to zero.

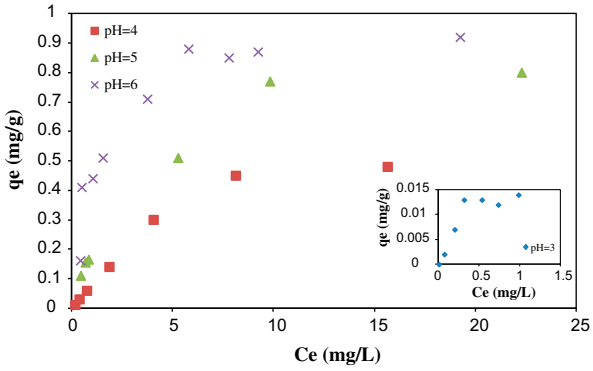

Fig. 6. Adsorption isotherm of virgin GAC at different pHs.

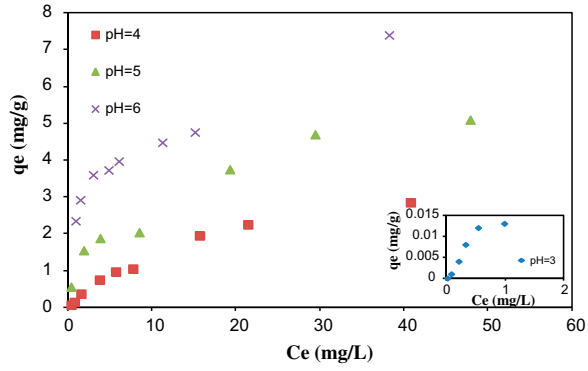

Fig. 7. Adsorption isotherm of GAC-NSIO(17%) at different pHs.

When $pH > pH_{pzc}$, the surface of adsorbent is negatively charged and can interact with positive substance, in contrast, when $pH < pH_{pzc}$, the surface of adsorbent is positively charged and can interact with negative substance.

Virgin GAC had a pH_{pzc} of 8.57, which means that its net surface charge was positive in the pH range of 3–6. Repulsion forces dominated between a positively charged GAC surface and the adsorbate which existed mainly as Cd^{2+}, $Cd(OH)^{+}$ [7] at the pH studied. This is manifested in the adsorption capacity. At pH 3, the repulsion force between GAC surface and adsorbate led to very little adsorption (close to none). As pH increased from 3 to 6, the repulsion force decreased as the positive surface charge gradually decreased and the adsorption capacity increased slightly.

On the basis of characterization results (pH_{pzc}, BET, TEM, XRD, XPS), GAC-NSIO(17%) have been proved to be successfully loaded by amorphous nanoscale iron oxides. And it had a pH_{pzc} of 9.84, which was in consistent with some previous research [38]. Similarly, its net surface charge was positive in the pH range of 3–6, interaction between surface and adsorbate which existed as Cd^{2}+, $Cd(OH)^{+}$ [7] formed repulsion force. This repulsion between the GAC-NSIO and Cd^{2+}(or $Cd(OH)^{+)}$ is also believed to be the mainly reason for change in adsorption capacity with the change of pH.

This is because in aqueous environment, nanoscale iron oxide particles are hydrated, and FeOH groups were fully formed in adsorbent surface [2]. FeOH groups stimulated the protonation and deprotonatioin process and formed $FeOH^{2+}$, FeOH, and FeO^{-}, whose fractions were mainly depended on solution pH [39]. $FeOH^{2+}$, FeOH, and FeO^{-} are dominant species at pH < 4, 4–9, and >9, respectively. When pH increased from 3 to 6, the positive intensity decreased accordingly although the net surface charge was still positive. $FeOH^{2+}$ was gradually converted to FeOH and H^{+} decreased accordingly. As seen in Fig. 7, the adsorption capacity was highest at pH 6, electrostatic attraction might have promoting effect to some extent.

Table 3
Adsorption isotherm constants for virgin GAC and GAC-NSIO(17%) at different pHs

		Langmuir isotherm model			Freundlich isotherm model		
Adsorbent	pH	q_{max} (mg/g)	b (L/mg)	R^2	K_f (mg/g)	$1/n$	R^2
Virgin GAC	3	0.01	5.64	0.94	0.01	0.34	0.59
	4	0.80	0.12	0.92	0.07	0.88	0.97
	5	0.91	0.30	0.99	0.19	0.47	0.93
	6	0.98	0.90	0.99	0.47	0.27	0.93
GAC-NSIO(17%)	3	0.02	2.98	0.99	0.02	0.55	0.96
	4	4.70	0.04	0.90	0.18	0.84	0.96
	5	5.86	0.12	0.95	0.91	0.46	0.96
	6	7.84	0.17	0.95	2.44	0.28	0.96

But, due to the still positive net surface, the electrostatic attraction might play a minor role.

At the same pH, though the net surface charge of GAC-NSIO(17%) was more positive than GAC, adsorption capacity of the former was much higher than the latter. This indicated that electrostatic attraction is not the only adsorption mechanism, other adsorption forces could exist. The potential adsorption mechanisms might include the following: (1) Donnan membrane effect: Non-diffusion sulfonate groups bound to GAC are non-specific for Cd(II) adsorption, due to the presence of $Fe_2(SO_4)_3$ as the precursor of nanoscale iron oxide and the addition of some sulfonate SO_4^{2-}groups into the surface and pores of adsorbent [19,20]. The sulfonate groups would enhance permeation and pre-enrichment of Cd(II) cations (such as Cd^{2+}, $Cd(OH)^+$) within the solid surface prior to sorption onto nanoscale iron oxide particles. This phenomenon is called as Donnan membrane effect which played a secondary role [20,34]. (2) Surface complexation: The removal of Cd(II) occurred in solutions having pH values less than the pH_{pzc} of GAC-NSIO(17%), and the electrostatic attraction played a minor role. Therefore, the most likely adsorption was specific adsorption through surface complexation with deprotonated process [40,41]. The possible process is shown below:

$$= FeOH + Cd^{2+} \leftrightarrow = FeO - Cd^{+} + H^{+} \quad (8)$$

$$= (FeOH)_2 + Cd^{2+} \leftrightarrow (= FeO)_2 - Cd^{+}2H^{+} \quad (9)$$

At pH 3, the degree of deprotonation of nanoscale iron oxide was lowest and adsorptive process hardly proceeded. Adsorption capacity was minimum (close to none). As pH increased from 3 to 6, the deprotonation degree of nanoscale iron oxide also increased, and the adsorption is more favorable, resulting in a significant increase in adsorption capacity.

In addition, iron concentration in the aqueous solution was also measured to study the stability of loaded nanoparticles during the experiments. No iron content was leaching at pH value of 4–6, when pH value was 3, only less than 0.25% of the loaded iron in GAC was dissolved into solution. This fully indicated that nanoscale iron oxide was very stable on the pores and surface of the material.

Finally, the adsorption capacity of GAC-NSIO (17%) was compared with various adsorbents reported in the literatures. The related data are listed in Table 4. It can been seen that GAC-NSIO(17%) exhibits excellent adsorption capacity of Cd(II) compared to other adsorbents.

3.4. Effect of contact time

The effect of contact time on Cd(II) adsorption by both adsorbents are shown in Fig. 8. Tables 5 and 6 list the adsorption kinetics constants and intraparticle diffusion model constants.

Compared with pseudo-first-order model, the adsorption data fitted well with the pseudo-second-order model, and the R^2 were 0.98 and 0.99, respectively. However, the loaded Fe had an adverse effect on the adsorption rate. The adsorption rate was 0.037 g/mg min for virgin GAC, but decreased to 0.013 g/mg min after loading iron oxides. This might be due to the fact that the loaded nanoscale iron oxide covered the pores and surface of GAC, which led to the restriction of Cd(II) diffusion to the specific adsorption sites and the adsorption rate was slowered.

K_d and C can be calculated from the slope and the intercept of the straight line of q_t vs. $t^{0.5}$. K_d is the rate constant, C represents the thickness of boundary layer. The higher the C value, the greater the boundary layer

Table 4
Comparison of the maximum adsorption capacity of Cd(II) by different adsorbent

Adsorbents	q_{max} (mg/g)	pH	Temperature (T)	References
Rice hull-activated carbon	0.84	5–8	293	[42]
Manganese oxide immobilized rice husk-activated carbon	3.58	5	298	[4]
Iron oxide immobilized rice husk-activated carbon	3.44	5	298	[4]
Manganese oxide immobilized nut waste activated carbon	2.64	5	298	[4]
Iron oxide immobilized nut waste activated carbon	2.87	5	298	[4]
Olive stone activated carbon	1.85	>6	293	[43]
Boehmite	3.55	6	298	[30]
Goethite	5.18	6	298	[30]
Natural sepiolite	0.28	–	–	[44]
GAC-NSIO(17%)	7.84	6	298	This study

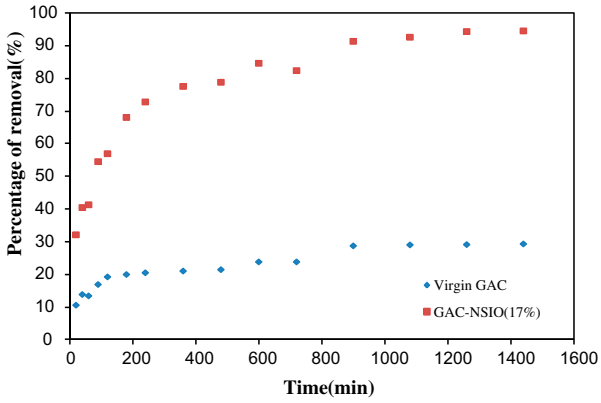

Fig. 8. Adsorption kinetics of virgin GAC and GAC-NSIO (17%).

Table 5
Adsorption kinetics constants of virgin GAC and GAC-NSIO(17%)

Adsorbent	Pseudo-first-order		Pseudo-second-order	
	K_1 (min^{-1})	R^2	K_2 (g/mg min)	R^2
Virgin GAC	0.0023	0.94	0.037	0.98
GAC-NSIO(17%)	0.003	0.97	0.013	0.99

effect. The plot of q_t against $t^{0.5}$ can form a straight line. If the line passed through the origin ($x = 0$, $y = 0$), the rate-limiting step is only due to the intraparticle diffusion. Otherwise, some other potential limiting steps along with intraparticle diffusion can be involved. According to Cheung et al. [45], in a solid–liquid adsorption process, the solute transfer is usually characterized by intraparticle diffusion, or external mass transfer (film diffusion), or both. There are three steps to analyze the mechanisms of adsorption: (1) transport of the Cd(II) from bulk solution through liquid film to the exterior surface of the adsorbent; (2) transport of the Cd(II) within the pores of the adsorbent where particle diffusion was rate limiting; (3) adsorption of the Cd(II) on the interior surface of the adsorbent. Previous results by other authors indicated that two or three steps were involved in the adsorption process [30]. As shown in Fig. 9, multilinearities were observed for two adsorbents, indicating not a purely intraparticle diffusion process and that three steps take place. The three regions in the q_t vs. $t^{0.5}$ plot suggest that the adsorption process proceeded by external surface adsorption (the initial linear region) which was completed in both cases within 180 min, intraparticle diffusion (the second linear region) and the adsorption of Cd(II) on the interior surface of the adsorbent (the third linear region).The last step is the final equilibrium step where intraparticle diffusion starts to slow down due to the low Cd(II) concentrations in the solutions. The intercept of the plot reflects the film diffusion effect and the larger of intercept, the greater the contribution of the surface adsorption in the rate-controlling step. The slope of the linear region of plot is the intraparticle diffusion parameter K_d. It is evident that the rate of external surface adsorption (step one) obtained for GAC-NSIO(17%) is much higher than virgin GAC for Cd(II) adsorption. The value of K_d, C, and R^2 are given in Table 6. Because all lines don't pass through the origin ($x = 0$, $y = 0$), some other potential limiting steps along with intraparticle diffusion are contributing to limit the adsorption rate.

3.5. Effect of temperature

ΔG°, ΔH°, and ΔS° values are calculated at 298 K for virgin GAC and GAC-NSIO(17%) to be -26.61 kJ/mol, 16.08 kJ/mol, and 0.14 kJ/mol K; -27.57 kJ/mol, 22.12 kJ/mol, and 0.18 kJ/mol K, respectively (Table 7).

The negative values of the Gibbs free energy change(ΔG°) indicates that the adsorption processes for both samples are thermodynamically feasible and spontaneous. The degree of spontaneity of the reaction increases with increasing temperature. Compared with virgin GAC, after the addition of nanoscale iron oxide in GAC-NSIO(17%), the negative value of ΔG° increased, indicating that it was more favorable to the spontaneous process. This increase of adsorptive capacity with temperature might be due to the increase in the active sites, and the decrease in the thickness of the boundary layer surrounding the GAC-NSIO(17%).

Table 6
Intraparticle diffusion model constants of virgin GAC and GAC-NSIO(17%)

Adsorbent	Intraparticle diffusion model								
	K_{d1}	K_{d2}	K_{d3}	C_1	C_2	C_3	R_1^2	R_2^2	R_3^2
Virgin GAC	0.0069	0.005	0.0004	0.0391	0.0459	0.1883	0.94	0.96	0.96
GAC-NSIO(17%)	0.0254	0.0092	0.003	0.0871	0.3115	0.5439	0.97	0.94	0.94

Table 7
Values of thermodynamic parameters for adsorption for virgin GAC and GAC-NSIO(17%)

Adsorbent	Temperature (K)	K_L L/mg)	ΔG° (kJ/mol)	ΔH° (kJ/mol)	ΔS° (kJ/mol K)
Virgin GAC	288	0.34	−25.28	16.08	0.14
	298	0.41	−26.61		
	308	0.53	−28.16		
GAC-*n*FeO(17%)	288	0.51	−26.25	22.12	0.18
	298	0.60	−27.57		
	398	0.94	−29.62		

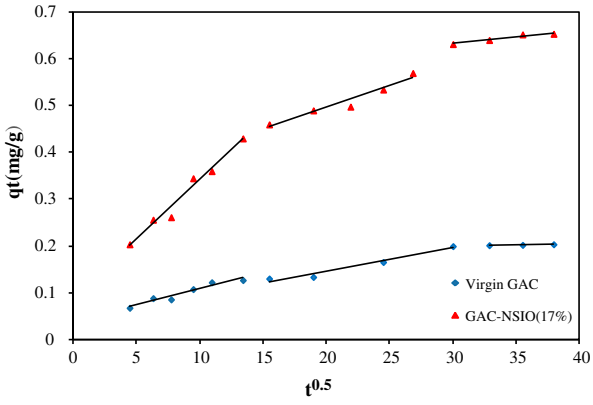

Fig. 9. Intraparticle diffusion kinetics for adsorption of virgin GAC and GAC-NSIO(17%).

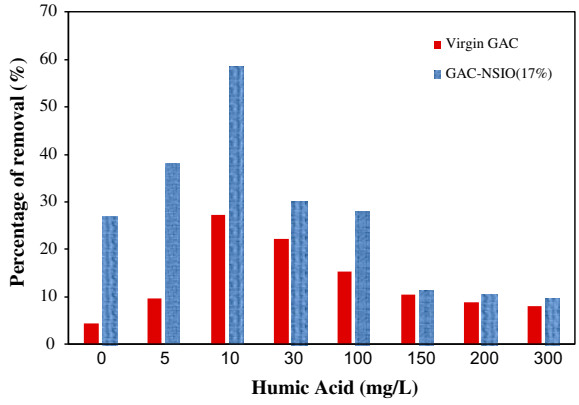

Fig. 10. Competitive adsorption between Cd(II) and humic acid for virgin GAC and GAC-NSIO(17%).

In general, ΔG° values up to 20 kJ/mol are consistent with electrostatic interaction (ion-exchange) between active sites and metal ion while ΔG° values more negative than 40 kJ/mol involve charge sharing or transfer from the adsorbent surface to the metal ion to form a coordinate bond [46]. The ΔG° values obtained in the study manifested that ion-exchange may play a significant role in the adsorption process, suggesting that a surface complexation reaction is the major mechanism responsible for Cd(II) adsorption process.

The positive values of enthalpy change (ΔH°) proved the endothermic nature of adsorption process. This results revealed that the consumption of amount of heat occurred to transfer the Cd(II) from liquid to solid phase, which may be explained by the reasons: (1) With increasing the temperature, the interaction between the active sites and Cd(II) occurred more easily; (2) The exchange between Cd(II) and H^+ needed to breaking the OH groups in the GAC-NSIO, which was an endothermic process; (3) In addition, Cd(II) diffusion process was also endothermic and the higher temperature favored the faster diffusion rate.

Generally, entropy change (ΔS°) was expected to be positive as to an adsorption reaction leads to transferring the adsorbate ions from disorderly state in the solution to a more ordered state when absorbed in the adsorbent. However, two important factors might have outweighed this decrease in the disorder: (1) The dehydration steps increased the mobility of the ions and that of the surrounding water molecules in the solution; (2) The larger number of species left the adsorbent when the adsorbate was exchanged for them. In particular, if the charge of the adsorbate exceeded the charge of the ions exchanged out of the adsorbent, the process was occurred more easily. For both materials, the positive entropy change (ΔS°) showed the affinity of adsorbent for Cd(II) and the increase of disorderliness, more mobility were generated in the reaction system. For GAC-NSIO(17%), due to the increase in the dehydration of Cd(II), Cd(II) would lose a large number of hydration water as to introduce to the surface of nanoscale iron oxide and Cd(II) would occur the ion-exchange process with the species in the GAC-NSIO to promote the decrease in the disorder [29,47].

In summary, although the nature of adsorption was not altered, the changes in thermodynamic parameter values (ΔG°, ΔH°, ΔS°) proved that the

loaded nanoscale iron oxide was favorable to Cd(II) adsorption.

3.6. Effect of humic acid

Naturally, humic acid (HA) and heavy metals exist simultaneously in water environment [48]. The adsorption capacity of Cd(II) by both adsorbents are studied in the presence of HA. The results are shown in Fig. 10. For virgin GAC, the adsorption capacity increased obviously with increasing concentration of HA from 0 to 10 mg/L, the highest percentage of removal was 27.2%. However, the adsorption capacity decreased gradually with the increasing concentration of HA from 10 to 300 mg/L. For GAC-NSIO(17%), the adsorption capacity increased obviously with increasing concentration of HA from 0 to 10 mg/L, the highest percentage of removal was 58.5%. However, the adsorption capacity decreased gradually with increasing concentration of HA from 10 to 300 mg/L. In summary, when concentrations of HA were in the range from 0 to 300 mg/L, the adsorption capacity of Cd(II) for GAC-NSIO(17%) were all much higher than virgin GAC.

For both adsorbents, in the low range concentrations (0~10 mg/L), HA had a promoting effect for adsorption process, but in the high range of concentrations (10~300 mg/L) HA had a inhibiting effect for adsorption process. This is because there are two possible reasons to explain this phenomenon in the Cd(II) adsorption process. (1) Inhibiting effect: HA and Cd(II) might both occupy the adsorption sites; the binding of HA with adsorbent would reduce the adsorption capacity of Cd(II) due to the competition. Meanwhile, HA might also inhibit Cd(II) adsorption through forming non-adsorbable complexes. (2) Promoting effect: Due to the formation of metal–ligand adsorbable complexes between HA and Cd(II), the adsorption capacity of Cd(II) could be significantly enhanced in the presence of HA [48,49].

3.7. Rapid small-scale column tests

The rapid small-scale column tests (RSSCTs) were employed and Fig. 11 illustrates the breakthrough curves of Cd(II) for both adsorbents. The results distinctly indicates that the GAC-NSIO(17%) can remove Cd(II) for much longer bed volumes (BVs) than the virgin GAC.

In general, when $C/C_0 = 0.9$ was achieved, it was considered that the column was penetrating and the adsorbent lost the adsorption capacity. GAC-NSIO (17%) and virgin GAC had about 1,120 BVs and 170 BVs, respectively. The former exhibited excellent adsorption capacity. This was because the loaded

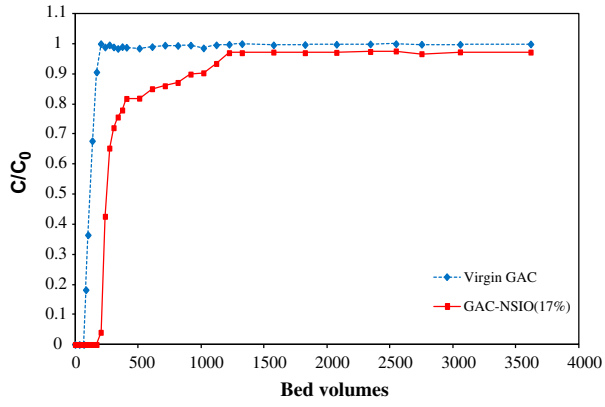

Fig. 11. Comparison of breakthrough curves of Cd(II) adsorption for virgin GAC and GAC-NSIO(17%) by two separate rapid small-scale column tests. ($C = 1$ mg/L, $T = 298$ K, pH = 6 and EBCT = 6 min.)

nanoscale iron oxides had well favorable affinity to Cd(II), and the change of pore size distribution had also advantageous effect for diffusion rates [19,25].

4. Conclusion

In this study, a potential adsorbent loaded with nanoscale iron oxide was prepared, characterized, and the adsorption capacity of Cd(II) was evaluated. Nanoscale iron oxide doped on GAC was proved to be effective in enhancing the adsorption capacity. The optimum loaded iron content was ~17%. Virgin GAC could only adsorb 0.98 mg Cd(II)/g, in contrast, the maximum adsorption capacity was 7.84 mg Cd(II)/g for GAC-NSIO(17%) under the same condition. The adsorption process was pH dependent, and high pH was more favorable. The stability of iron loaded was excellent in the pH range of 3–6. Cd(II) adsorption was an adsorption process of endothermic nature. The presence of humic acid had an interesting effect on adsorption: promoting at low concentrations (1–10 mg/L) and inhabiting at high concentrations (10–300 mg/L). Rapid small-scale column tests also proved that GAC-NSIO(17%) had an excellent adsorption capacity of Cd(II), compared with virgin GAC. The main adsorption mechanism was surface complexation, in addition, the electrostatic attraction and Donnan membrane effect also had contribution to Cd(II) adsorption.

Acknowledgment

This work was supported by Shanghai Science and Technology Development Fund for Environmental Protection (no. 2012-03).

References

[1] Z.H. Yu, X.D. Zhang, Y.M. Huang, Magnetic chitosan–iron(III) hydrogel as a fast and reusable adsorbent for chromium(VI) removal, Ind. Eng. Chem. Res. 52 (2013) 11956–11966.

[2] M.A. Ahmed, S.M. Ali, S.I. El-Dek, A. Galal, Magnetite-hematite nanoparticles prepared by green methods for heavy metal ions removal from water, Mater. Sci. Eng. B 178 (2013) 744–751.

[3] A. Agrawal, K.K. Sahu, Kinetic and isotherm studies of cadmium adsorption on manganese nodule residue, J. Hazard. Mater. 137 (2006) 915–924.

[4] S.M. Lee, Lalhmunsiama, S.I. Choi, D. Tiwari, Manganese and iron oxide immobilized activated carbons precursor to dead biomasses in the remediation of cadmium-contaminated waters, Environ. Sci. Pollut. R. 20 (2013) 7464–7477.

[5] L. Jarup, A. Akesson, Current status of cadmium as an environmental health problem, Toxicol. Appl. Pharm. 238 (2009) 201–208.

[6] R. Schutte, T.S. Nawrot, T. Richart, L. Thijs, D. Vanderschueren, T. Kuznetsova, E. Van Hecke, H.A. Roels, J.A. Staessen, Bone resorption and environmental exposure to cadmium in women: A population study, Environ. Health Persp. 116 (2008) 777–783.

[7] S.M. Lee, C. Laldawngliana, D. Tiwari, Iron oxide nano-particles-immobilized-sand material in the treatment of Cu(II), Cd(II) and Pb(II) contaminated waste waters, Chem. Eng. J. 195 (2012) 103–111.

[8] Q. Chen, Z. Luo, C. Hills, G. Xue, M. Tyrer, Precipitation of heavy metals from wastewater using simulated flue gas: Sequent additions of fly ash, lime and carbon dioxide, Water Res. 43 (2009) 2605–2614.

[9] A. Olad, S. Ahmadi, A. Rashidzadeh, Removal of Nickel (II) from aqueous solutions with polypyrrole modified clinoptilolite: kinetic and isotherm studies, Desalin. Water Treat. 51 (2013) 7172–7180.

[10] N. Chaouch, M.R. Ouahrani, S. Chaouch, N. Gherraf, Adsorption of cadmium (II) from aqueous solutions by activated carbon produced from Algerian dates stones of Phoenix dactylifera by H_3PO_4 activation, Desalin. Water Treat. 51 (2013) 2087–2092.

[11] H. Al-Zoubi, A. Rieger, P. Steinberger, W. Pelz, R. Haseneder, G. Hartel, Nanofiltration of acid mine drainage, Desalin. Water Treat. 21 (2010) 148–161.

[12] X.Z. Yuan, Y.T. Meng, G.M. Zeng, Y.Y. Fang, J.G. Shi, Evaluation of tea-derived biosurfactant on removing heavy metal ions from dilute wastewater by ion flotation, Colloids Surf., A 317 (2008) 256–261.

[13] S. Bayar, A.E. Yilmaz, R. Boncukcuoglu, B.A. Fil, M.M. Kocakerim, Effects of operational parameters on cadmium removal from aqueous solutions by electrochemical coagulation, Desalin. Water Treat. 51 (2013) 2635–2643.

[14] L. Sun, E. Miznikov, L. Wang, A. Adin, Nickel removal from wastewater by electroflocculation–filtration hybridization, Desalination 249 (2009) 832–836.

[15] P.A. Xu, G.M. Zeng, D.L. Huang, C.L. Feng, S. Hu, M.H. Zhao, C. Lai, Z. Wei, C. Huang, G.X. Xie, Z.F. Liu, Use of iron oxide nanomaterials in wastewater treatment: A review, Sci. Total Environ. 424 (2012) 1–10.

[16] J.L. Gong, B. Wang, G.M. Zeng, C.P. Yang, C.G. Niu, Q.Y. Niu, W.J. Zhou, Y. Liang, Removal of cationic dyes from aqueous solution using magnetic multi-wall carbon nanotube nanocomposite as adsorbent, J. Hazard. Mater. 164 (2009) 1517–1522.

[17] A.D. Abid, M. Kanematsu, T.M. Young, I.M. Kennedy, Arsenic removal from water using flame-synthesized iron oxide nanoparticles with variable oxidation states, Aerosol Sci. Tech. 47 (2013) 169–176.

[18] L. Giraldo, A. Erto, J.C. Moreno-Pirajan, Magnetite nanoparticles for removal of heavy metals from aqueous solutions: Synthesis and characterization, Adsorption 19 (2013) 465–474.

[19] J. Xu, N. Gao, Y. Deng, S. Xia, Nanoscale iron hydroxide-doped granular activated carbon (Fe-GAC) as a sorbent for perchlorate in water, Chem. Eng. J. 222 (2013) 520–526.

[20] B.J. Pan, H. Qiu, B.C. Pan, G.Z. Nie, L.L. Xiao, L. Lv, W.M. Zhang, Q.X. Zhang, S.R. Zheng, Highly efficient removal of heavy metals by polymer-supported nanosized hydrated Fe(III) oxides: Behavior and XPS study, Water Res. 44 (2010) 815–824.

[21] M.K. Doula, Simultaneous removal of Cu, Mn and Zn from drinking water with the use of clinoptilolite and its Fe-modified form, Water Res. 43 (2009) 3659–3672.

[22] A. Erto, L. Giraldo, A. Lancia, J.C. Moreno-Piraján, A comparison between a low-cost sorbent and an activated carbon for the adsorption of heavy metals from water, Water, Air, & Soil Pollution 224 (2013) 1531–1540.

[23] W. Liu, J. Zhang, C. Zhang, L. Ren, Preparation and evaluation of activated carbon-based iron-containing adsorbents for enhanced Cr(VI) removal: Mechanism study, Chem. Eng. J. 189–190 (2012) 295.

[24] Z. Gu, J. Fang, B. Deng, Preparation and evaluation of GAC-based iron-containing adsorbents for arsenic removal, Environ. Sci. Technol. 39 (2005) 3833–3843.

[25] M. Jang, W.F. Chen, F.S. Cannon, Preloading hydrous ferric oxide into granular activated carbon for arsenic removal, Environ. Sci. Technol. 42 (2008) 3369–3374.

[26] S. Nethaji, A. Sivasamy, A.B. Mandal, Preparation and characterization of corn cob activated carbon coated with nano-sized magnetite particles for the removal of Cr(VI), Bioresour. Technol. 134 (2013) 94–100.

[27] W.F. Chen, R. Parette, J.Y. Zou, F.S. Cannon, B.A. Dempsey, Arsenic removal by iron-modified activated carbon, Water Res. 41 (2007) 1851–1858.

[28] Y.H. Chen, F.A. Li, Kinetic study on removal of copper(II) using goethite and hematite nano-photocatalysts, J. Colloid Interf. Sci. 347 (2010) 277–281.

[29] E. Eren, H. Gumus, Characterization of the structural properties and Pb(II) adsorption behavior of iron oxide coated sepiolite, Desalination 273 (2011) 276–284.

[30] F. Granados-Correa, N.G. Corral-Capulin, M.T. Olguín, C.E. Acosta-León, Comparison of the Cd(II) adsorption processes between boehmite (γ-AlOOH) and goethite (α-FeOOH), Chem. Eng. J. 171 (2011) 1027–1034.

[31] J.S. Noh, J.A. Schwarz, Effect of HNO_3 treatment on the surface acidity of activated carbons, Carbon 28 (1990) 675–682.

[32] Z.C. Kadirova, K. Katsumata, T. Isobe, N. Matsushita, A. Nakajima, K. Okada, Adsorption and photodegradation of methylene blue by iron oxide impregnated on granular activated carbons in an oxalate solution, Appl. Surf. Sci. 284 (2013) 72–79.

[33] G. Muñiz, V. Fierro, A. Celzard, G. Furdin, G. Gonzalez-Sánchez, M.L. Ballinas, Synthesis, characterization and performance in arsenic removal of iron-doped activated carbons prepared by impregnation with Fe(III) and Fe (II), J. Hazard. Mater. 165 (2009) 893–902.
[34] Q. Zhang, B. Pan, X. Chen, W. Zhang, B. Pan, Q. Zhang, L. Lv, X.S. Zhao, Preparation of polymer-supported hydrated ferric oxide based on Donnan membrane effect and its application for arsenic removal, Sci. China, Ser. B 51 (2008) 379–385.
[35] M.K. Doula, Synthesis of a clinoptilolite–Fe system with high Cu sorption capacity, Chemosphere 67 (2007) 731–740.
[36] S.R. Qiu, H.F. Lai, M.J. Roberson, M.L. Hunt, C. Amrhein, L.C. Giancarlo, G.W. Flynn, J.A. Yarmoff, Removal of contaminants from aqueous solution by reaction with iron surfaces, Langmuir 16 (2000) 2230–2236.
[37] Y. Gao, Y.J. Kim, S.A. Chambers, Preparation and characterization of epitaxial iron oxide films, J. Mater. Res. 13 (1998) 2003–2014.
[38] N. Boujelben, J. Bouzid, Z. Elouear, Adsorption of nickel and copper onto natural iron oxide-coated sand from aqueous solutions: Study in single and binary systems, J. Hazard. Mater. 163 (2009) 376–382.
[39] L. Cumbal, A.K. Sengupta, Arsenic removal using polymer-supported hydrated iron(III) oxide nanoparticles: role of Donnan membrane effect, Environ. Sci. Technol. 39 (2005) 6508–6515.
[40] T. Phuengprasop, J. Sittiwong, F. Unob, Removal of heavy metal ions by iron oxide coated sewage sludge, J. Hazard. Mater. 186 (2011) 502–507.
[41] A. Zach-Maor, R. Semiat, H. Shemer, Removal of heavy metals by immobilized magnetite nano-particles, Desalin. Water Treat. 31 (2011) 64–70.
[42] M. Teker, M. Imamoglu, O. Saltabas, Adsorption of copper and cadmium ions by activated carbon from rice hulls, Turk. J. Chem. 23 (1999) 185–191.
[43] I. Kula, M. Uğurlu, H. Karaoğlu, A. Çelik, Adsorption of Cd(II) ions from aqueous solutions using activated carbon prepared from olive stone by $ZnCl_2$ activation, Bioresour. Technol. 99 (2008) 492–501.
[44] S. Kocaoba, Adsorption of Cd(II), Cr(III) and Mn(II) on natural sepiolite, Desalination 244 (2009) 24–30.
[45] W.H. Cheung, Y.S. Szeto, G. McKay, Intraparticle diffusion processes during acid dye adsorption onto chitosan, Bioresour. Technol. 98 (2007) 2897–2904.
[46] C.H. Weng, C.Z. Tsai, S.H. Chu, Y.C. Sharma, Adsorption characteristics of copper(II) onto spent activated clay, Sep. Purif. Technol. 54 (2007) 187–197.
[47] E. Eren, H. Gumus, N. Ozbay, Equilibrium and thermodynamic studies of Cu(II) removal by iron oxide modified sepiolite, Desalination 262 (2010) 43–49.
[48] W.W. Tang, G.M. Zeng, J.L. Gong, J. Liang, P. Xu, C. Zhang, B.B. Huang, Impact of humic/fulvic acid on the removal of heavy metals from aqueous solutions using nanomaterials: A review, Sci. Total Environ. 468–469 (2014) 1014–1027.
[49] C.H. Lai, C.Y. Chen, Removal of metal ions and humic acid from water by iron-coated filter media, Chemosphere 44 (2001) 1177–1184.